MEASUREMENT OF ELASTIC-PLASTIC STRAINS AROUND NOTCHES USING DIC TECHNIQUES

Rafael Cesar de O. Góes, rafael.goes@petrobras.com
Leonardo Dantas Rodrigues, leodr@aluno.puc-rio.br
Mechanical Engineering Department, PUC-Rio

Jaime de Castro Neto, jcastro@tecgraf.puc-rio.br
Tecgraf, PUC-Rio

Jaime Tupiassú Pinho de Castro, jtcastro@puc-rio.br
José Luiz de França Freire, jlfreire@puc-rio.br
Mechanical Engineering Department, PUC-Rio

Luiz Fernando Martha, lfm@tecgraf.puc-rio.br
Civil Engineering Department, PUC-Rio

Abstract. *This work studies full-field distributions of elastic-plastic strains around notches by comparing experimental measurements made using up-to-date digital image correlation techniques and finite element numerical predictions. Initially, some instability problems in elastic-plastic finite element predictions are illustrated, and a few fundamental concepts of the digital image correlation technique are briefly introduced. Then the experiment is presented, describing how a steel plate with a circular hole is progressively pulled beyond the elastic limit, being photographed at every load step. Through digital image correlation techniques, the strain fields close to the hole are calculated from the successively measured displacement fields around the notch tip. Then, the stress-strain curve of the plate material is obtained and used in an elastic-plastic finite element model. Finally, the finite element solution is compared with measured strain fields, and with predictions made by Neuber and by Molski-Glynka stress/strain concentration rules.*

Keywords*: Digital Image Correlation, elastic-plastic strains, Finite Element, strain concentration rules.*

1. INTRODUCTION

Mathematical modeling of structural components behavior under elastic-plastic (EP) loads can present difficulties both from analytical and from numerical points of view. Whereas several analytical solutions for linear elastic (LE) stress analysis problems are available to be used as reference cases to check predictions made by finite element (FE) models, EP analytical reference solutions are scarce and, when available, usually do not consider strain hardening effects thus cannot reproduce well but limit load problems. Therefore, EP stress and strain field numerical predictions must be frequently made without such analytical references, meaning that the structural designer must rely on results that cannot be easily checked. Indeed, for example in low-cycle fatigue analysis, classical semi-empirical formulas for predicting stress/strain concentration effects at notch roots, such as Neuber, Linear, and Molski-Glinka rules, are widely used to estimate them under EP conditions. But they cannot be used to predict stress and strain fields around the notch roots, nor can be analytically verified. Moreover, as the superposition principle cannot be used in EP problems, the much helpful trick of subdividing them in simpler problems cannot be used in practical applications. Powerful Finite element (FE) codes are certainly available to tackle such problems, but they are not as robust as they should, particularly when dealing with high strain gradients or near-plastic collapse problems.

Such differences are exemplified in Figure 1, which shows different predictions for the maximum EP strain in the border of a circular hole in an infinite plate of elastic-perfectly plastic material under uniaxial stress. The FE analysis was performed with the best resources available, but it become unstable after 80% of the plastic collapse load. It is worth to present some details used in this analysis. A plane stress finite element model was built in ANSYS 11.0, representing its ¼ symmetry. An elastic-perfectly plastic material model was assumed. Two types of mesh, triangular and quadrilateral, were used to discretize the plate, both of them using PLANE183 element from the ANSYS library. PLANE183 is a higher order element suited for irregular faces. Each node has two degrees of freedom (displacements in *x* and *y* directions), and a simple switch-key option that can turn the element shape from 8-node quadrilateral (or degenerated triangle) to 6-node triangle, see Figure 2. In both meshes the same refinement rule was applied, imposing an element size close to 1/40 of the hole radius at the notch root, and a smooth increase from this point on.

Symmetry boundary condition was applied in *x* and *y*-axis. The nominal stress was applied as uniform pressure on the far up boundary, while the right boundary was left free to move, avoiding Poisson's effect and maintaining the plate uni-axially loaded. Large displacements hypothesis was assumed. The load was increased in small steps up to $\sigma_n = S_Y$, where σ_n is the nominal stress applied on the plate, and S_Y is the material yield strength. The performed runs presented an unstable behavior for the FE predicted notch behavior under high loads, as shown in Figure 1: note the divergence on the predicted strains for $\sigma_n > 0.8S_Y$. Figure 2 shows the predicted strain profile.

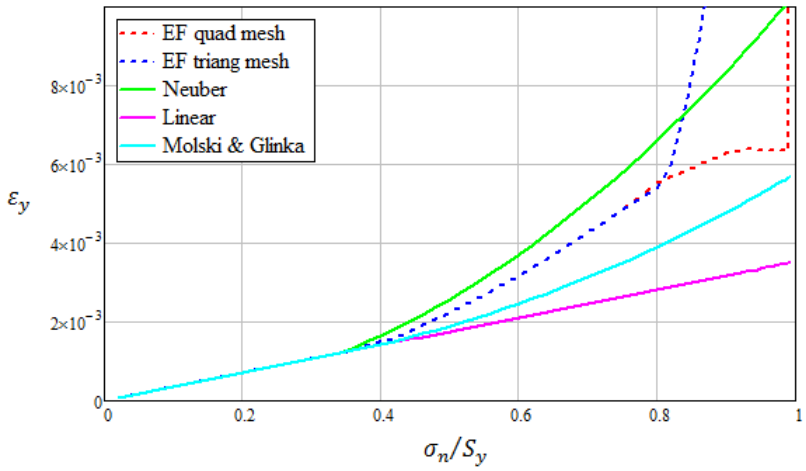

Figure 1: ε_y strain component at the notch root predicted by FE EP analysis, and by strain concentration rules.

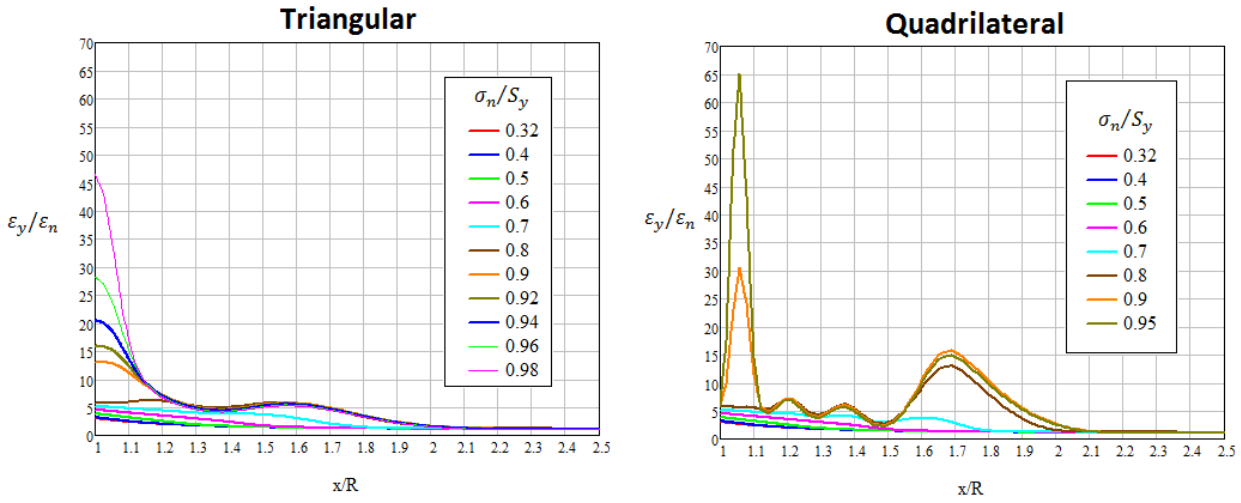

Figure 2: Strain profiles departing from the notch root predicted using different elements.

These figures show that the material at the notch root stopped working in the quadrilateral mesh, forcing the strain concentration point to move to the interior of the plate. At the same time, the triangular mesh did not present this behavior, as the strain in the notch root rapidly increased after $\sigma_n > 0.8S_Y$. The stress and strain fields were monitored after every run against boundary effects, as an infinite domain cannot be represented in the Finite Elements Method. Continuous checks confirmed that the used width and height of the ¼ plate model (40·R) were enough to prevent the hole neighborhood from boundary effects.

Later, the material was changed from elastic-perfectly plastic to bilinear. In the bilinear material, the stress-strain curve is composed by two linear segments with independent slopes: the elasticity modulus E from $\sigma = 0$ to $\sigma = S_Y$, and a second modulus E', from the yield stress on. E' = 0 reproduces the elastic-perfectly plastic model. For E' = E the material behaves as linear elastic. Values in between those extremes reproduce an increasing strain hardening capability. Figure 3 illustrates the predicted EP frontiers for $\sigma_n = 0.8S_Y$. It can be observed in this figure that the lower the E' value, the larger the plastic zone is. Also, as E' decreases, the plastic zone gets progressively thinner and more elongated, projecting itself into the piece. The plastic zones predicted for E' = 0.1·E and for E' = 0.2·E presented irregular shapes because they invaded a less refined mesh, but their general aspect is not compromised.

To verify such predictions, strain gages can surely be used to measure the EP stress/strain concentration behavior at suitable notch roots, even thou these measurements are far from trivial. However, this challenging experimental problem is considered beyond the scope of this paper. Nevertheless, it is important to mention that strain gages are local sensors, which cannot be used to obtain full field information. Moreover, their finite size can be an important obstacle in high strain gradient fields. Indeed, the measured strains must be numerically corrected to reflect the strain variations under the gage area, a non-trivial task if the gages objective is to measure such variations. Such difficulties in obtaining reliable experimental data for elastic-plastic strain fields around notches for comparison with predictions is one of the

main obstacles to adequately adjust and validate either analytical or numerical models. The relatively new DIC technique has been shown to be potentially useful for the determination of full-field strain fields, including those around notches (Sutton et al, 2009). This potential is explored in this work. Furthermore, the present work has two other more precise objectives: to compare the elastic-plastic strain fields obtained through Finite Element modeling and from measurements based on the DIC technique, in a relatively simple piece with a well controlled strain gradient, and to verify both results against Neuber and Molski-Glinka models predictions (Castro and Meggiolaro, 2009).

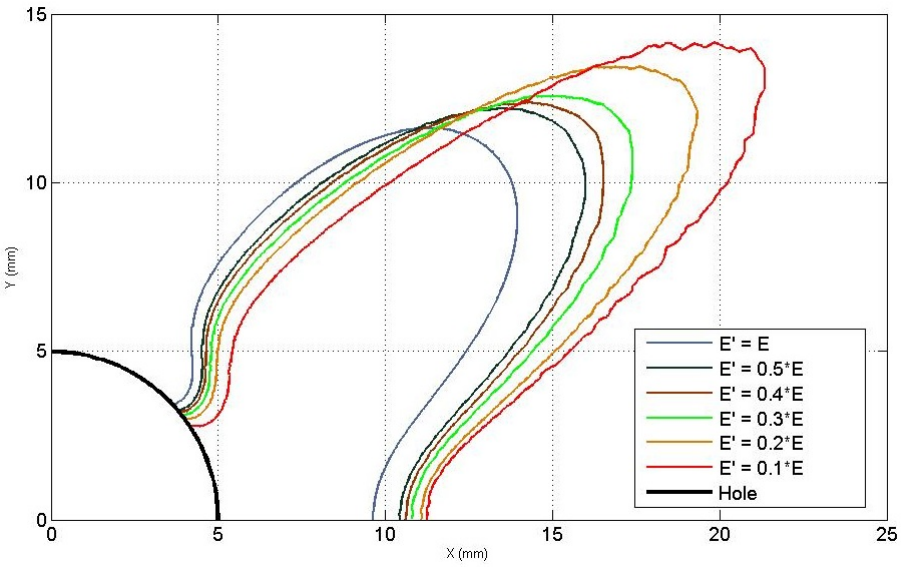

Figure 3. Plastic zones frontiers predicted for $\sigma_n = 0.8S_Y$.

2. FUNDAMENTALS OF THE DIC TECHNIQUE

Digital Image Correlation (DIC) is an advanced optical-numerical full-field displacement measurement technique, which is nowadays widely used for tackling several problems in experimental mechanics. For EP strain analysis in particular, proper equations should be used to correlate displacement measurements with the resulting strain fields, see for example Sutton et al (2009). In essence, this technique is based in elaborated comparisons between pictures taken during different loading stages of a properly prepared sample. With modern equipment, strain field measurements require the region of measurement to be covered by a cloud of dots distributed randomly over a highly contrasting base. Suitable bases can be obtained for example by covering the structural component surface with a uniform white paint (which should be sufficiently ductile for EP strain fields measurements), while the black dots can be inserted by spray painting it with a pressurized canned paint, an air brush, or other similar techniques (graphite sprays used for lubrication may be a viable option, e.g.). Ideally, the dot's size should fully cover one pixel and somewhat affect the light intensity of a group of 3x3 adjacent pixels. The density of about 1 dot for each square of 3x3 pixels leads to the use of subset sizing, for example 16x16 or 41x41 pixels that contain about and respectively 30 or 90 dots (Shukla and Dally, 2010). The technique aims to determine the average displacements of the subset centers between the initial and final images, or between subsequent images in step-load measurements.

Equation (1) shows one possible correlation function that can be used to identify the subset matching where $F(x, y)$ and $G(x^*, y^*)$ represent the gray levels (light intensities) of each point (x, y) or (x^*, y^*) inside the un-deformed or deformed subset. The best matching fit is given by the maximum value of the cross-correlation function defined by

$$C(x, y, x^*, y^*) = \frac{\sum F(x, y).G(x^*, y^*)}{\sqrt{\sum F(x, y)^2 . \sum G(x^*, y^*)^2}} \tag{1}$$

The distribution of gray level from pixel to pixel is a discrete function. Continuous gray level distributions can be achieved for both images if the pixel by pixel gray level distributions can be smoothed out by some kind of interpolation function. The best search to achieve a maximum value for C or a minimum value for $(1 - C)$ determines the coordinate pair (x^*, y^*) expressed by an approximating series, such that

$$x^* = x + u + \frac{\partial u}{\partial x}.\Delta x + \frac{\partial u}{\partial y}.\Delta y + ... \qquad (2)$$
$$y^* = y + v + \frac{\partial v}{\partial x}.\Delta x + \frac{\partial v}{\partial y}.\Delta y + ...$$

where only the linear terms were explicitly written. Achievement of the best correlation will provide the set of terms $u, v, \frac{\partial u}{\partial x}, \frac{\partial v}{\partial x}, \frac{\partial u}{\partial y}, \frac{\partial v}{\partial y}$ that make possible the determination of the strain state ε_x, ε_y, ε_{xy}. In these cases, expressions for small or large strains can be used. Minimization of the expression $1 - C(x, y, x^*, y^*)$ may be achieved by using the Newton-Raphson method (Sutton, Orteu and Schreier, 2009).

Calibration of the stereovision system is performed using a precision reference plate with dimensions similar to the area of interest, with a known speckle dot pattern. The calibration plate should be positioned in front of the cameras at the same point where the specimen will be positioned during the test. Several images should be obtained while the reference plate is rotated and translated randomly. It is recommended a minimum of twenty images for a reliable calibration (Yan et al., 2007). Table 1 shows some stereovision parameters obtained by the calibration performed for the measurements made in this investigation.

Table 1. Calibration parameters of the stereovision system

Overall score: 0.067 * Camera 1 residual score: 0.049 Camera 2 residual score: 0.06	
*The manual of equipment deemed the calibration acceptable for overall values below 0.1 (VIC-3D Manual, 2009)	
Camera 0 intrinsics (distances in pixels): Center (X): 1117.32 Center (Y): 1209.8 Focal Length (X): 20040.8 Focal Length (Y): 20040.8 Skew: -4.187 Kappa 1: -0.092 Kappa 2: 50.426	Camera 1 intrinsics (distances in pixels): Center (X): 1280.369 Center (Y): 1070.995 Focal Length (X): 20634.186 Focal Length (Y): 20634.239 Skew: -6.173 Kappa 1: 0.186 Kappa 2: -18.033
where: - skew is the deviation from orthogonality between the row and column directions in the sensor plane; - Kappa is the radial distortion coefficient;	

3. EXPERIMENTAL MODEL

The experimental specimen was a normalized SAE 1020 steel plate with a relatively large central hole, whose dimensions are schematized in Figure 4. To avoid indentation problems at the pulling holes, the upper and lower plate edges were reinforced by a welded bar, not shown in the figure. The analysis area in the plate was first painted with an adequate white paint and then gently sprayed with a black paint, to create the random highly contrasting dots distribution that forms the speckle pattern appropriate for the DIC system (Figure 5). The equipment used for the DIC analysis was a VIC2009 commercial system provided by Correlated Solutions. It consists of two monochromatic digital cameras, a set of professional lenses, precision calibration standards, appropriate tripods and supporting hardware, and a high performance software. The tensile loads were applied in a 100kN servo-hydraulic Instron machine, under load control, a necessary precaution since the 1020 steel is strain rate sensitive and presents some relaxation under plastic loads (Ach et al, 2010). The plate was initially submitted to incremental loads of 10 kN, until reaching 40KN. This incremental load step was then gradually reduced until reaching 1KN from 52KN (near the initial plasticization of the notch tip) up to the final 70KN load used for this analysis.

This model was chosen to verify if such a configuration could be used as a reference to stress concentration EP problems, like the one described in the introduction. Thus it first was loaded under LE conditions to verify the experimental set-up behavior and to estimate the overall measurement uncertainty, unloaded, and then reloaded for the EP strain field measurements. The various load steps were photographed twice, to verify possible sources of experimental dispersion. Then the whole set of photos was sequentially analyzed by the DIC software, to calculate the displacement fields induced by the various load steps, and from then the resulting strain fields. Using a high-performance microcomputer (Core i7 with 6Gb RAM, 1Tb HD, G-Force GTX 220 graphic card with 1Gb memory), each analysis required about a couple of minutes to be performed.

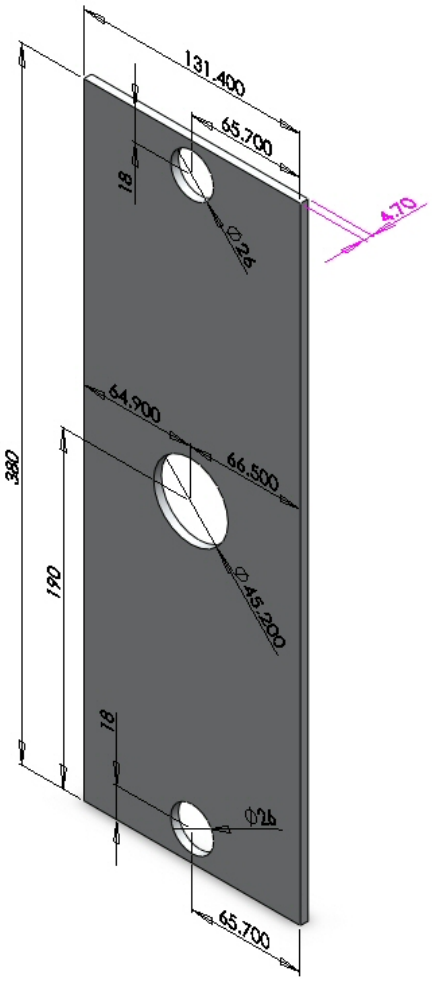

Figure 4: Specimen dimensions

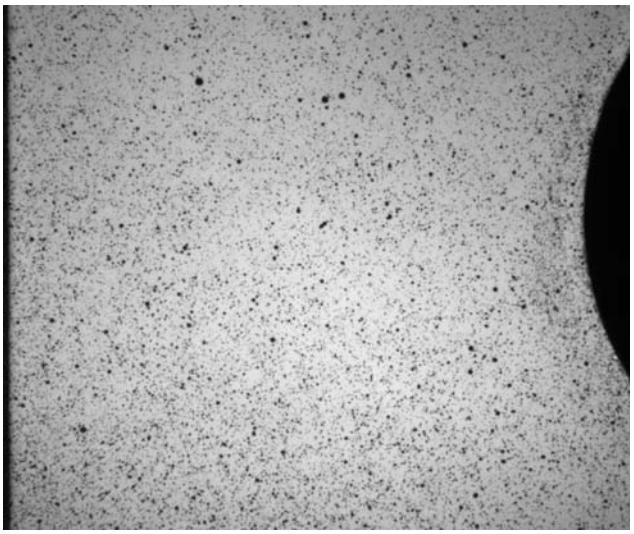

Figure 5: Speckle pattern in the analysis region.

4. FINITE ELEMENT MODEL

A detailed plane stress finite element model of the tested plate was built using the Abaqus FE software. The geometry, representing 1/2 of symmetry, was discretized with CPS4R and CPS3 elements from the Abaqus library, respectively 4 and 3-node linear elements. Each node has two degrees of freedom (displacements in *x* and *y* directions).

The model had essentially two parts: the plate and the reinforcement. As there was no interest in the stresses around the reinforcement, no particular attention was paid to its mesh. Also, being much thicker, the reinforcement was modeled with a higher elasticity's module than the plate, to avoiding the need for a 3D model. The plate itself received a finer mesh, especially in the proximities of the hole. A total of approximately 34000 elements were used. Figures 6(a) and 6(b) show the general aspect of the meshed model.

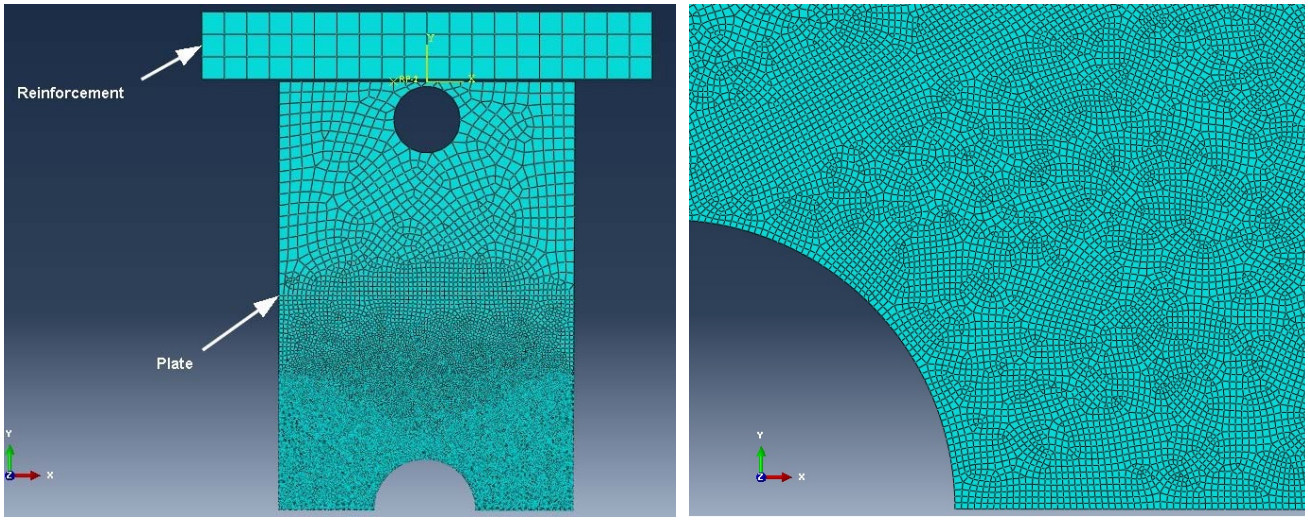

(a) (b)

Figure 6: Finite Elements mesh at the whole plate (a), and close to the hole (b).

A multi-linear material model was used to describe the material behavior, adapted from data obtained in a tensile test. Both parts were tied together with bonded contact, allowing no relative displacement of the nodes in their interface.

Symmetry boundary condition was applied in *x*-axis. The test load was applied as a uniform pressure *p* on the pin diameter projection on the reinforcement.

$$p = \frac{P}{d_{pin} \cdot t} \tag{3}$$

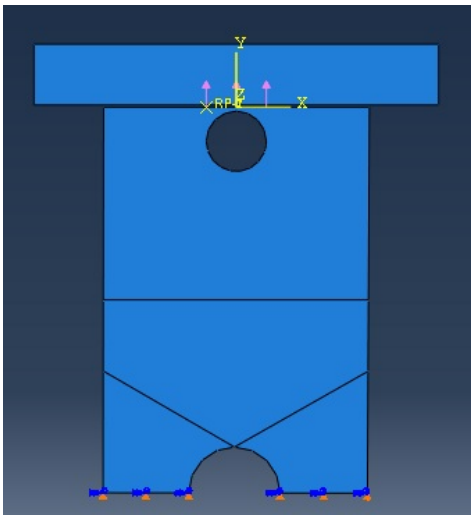

Figure 7: Model with boundary conditions applied

Small displacements hypothesis was assumed, and the load was increased up to 70kN in small increments, using direct equation solver and a Full-Newton solution technique.

5. RESULTS AND DISCUSSIONS

Figure 8(a) show the aspect of the maximum strain (ε_{yy}) field close to the notch root predicted by the finite elements model, and Figure 8(b) the field measured by the DIC equipment under EP conditions. The strain gradients in radial and circumferential directions are similar in both solutions. Also, both find themselves qualitatively within the expected values for the employed geometry and load, estimated by analytical approximations based on the Kirsh solution.

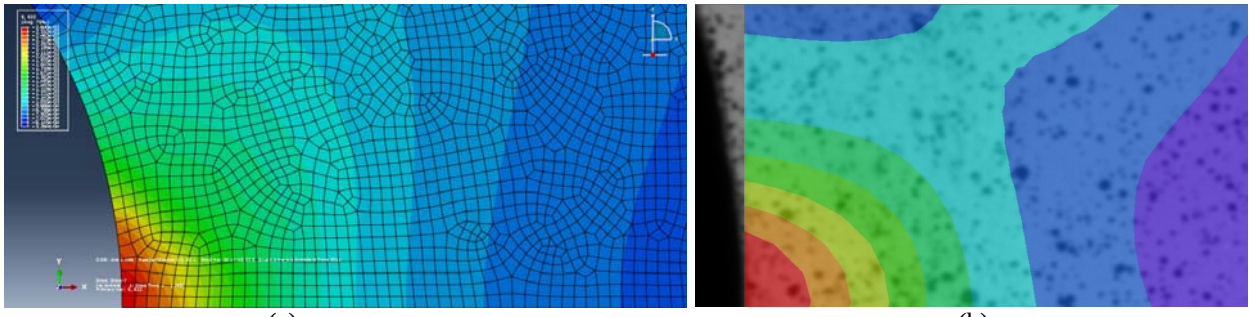

(a) (b)

Figure 8: Strain gradients in radial and circumferential directions by FE (a) and DIC (b)

In Figure 9, the ε_{yy} profiles predicted by finite element and measured by the DIC system in the plate residual ligament are compared for several load levels. Figure 10 shows the comparison of DIC and FE results at similar points of the specimen for all loadings. Table 2 shows information regarding the differences between the results obtained from the DIC measurements and from the FE analysis. As shown in Figure 10, the overall agreement between FE predictions and DIC measurements in this case was quite reasonable.

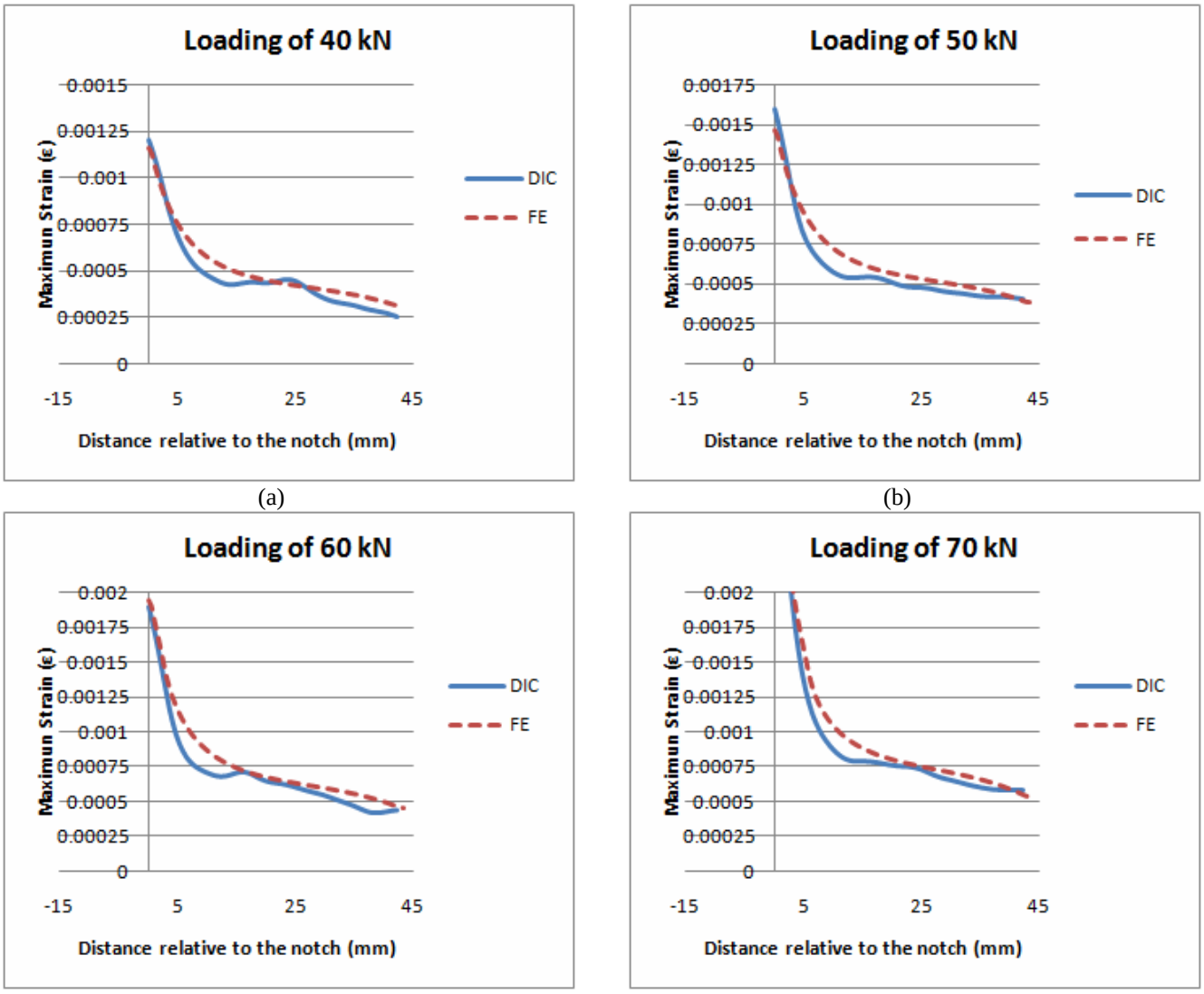

(a) (b)

(c) (d)

Figure 9: Predicted and measured maximum strain (ε_{yy}) for loads of 40, 50, 60 and 70 kN.

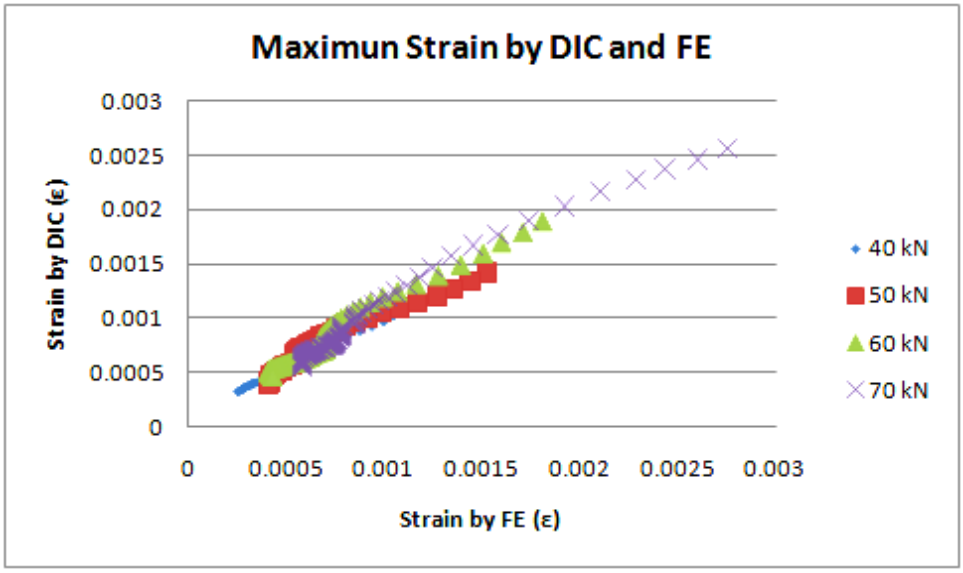

Figure 10: Comparison of DIC and FE results at similar points of the specimen for all loadings.

Table 2: Differences between DIC measurements and FE predictions.

Load (kN)	Avarage Deviation (DIC-FE) (με)	Root Mean Square (με)	Maximum Deviation (DIC-FE) (με)
40	-46	40	-227
50	-56	55	-220
60	-85	58	-148
70	-63	73	-105
All loads	-62	60	-

In higher strain gradient regions, errors of larger magnitude were expected both for the numerical model, whose difficulties were commented in the introduction, as well as for the experimental results, since these regions are very sensitive to the DIC parameters chosen for these measurements.

The greater differences between the strain values found at points where the gradients are smaller may explain the sensitivity of the DIC technique to the pattern of speckles inserted into the specimen. Figure 10 demonstrates that strains independently calculated by both techniques coincided satisfactorily. This can be demonstrated by the proximity of the data points to a 45° line.

Figure 11 compares the ε_{yy} strain at the notch root obtained by Finite Elements, DIC, Neuber and Molski & Glinka predictions. From 50kN on, EF and Neuber predictions indicate significative plastification.

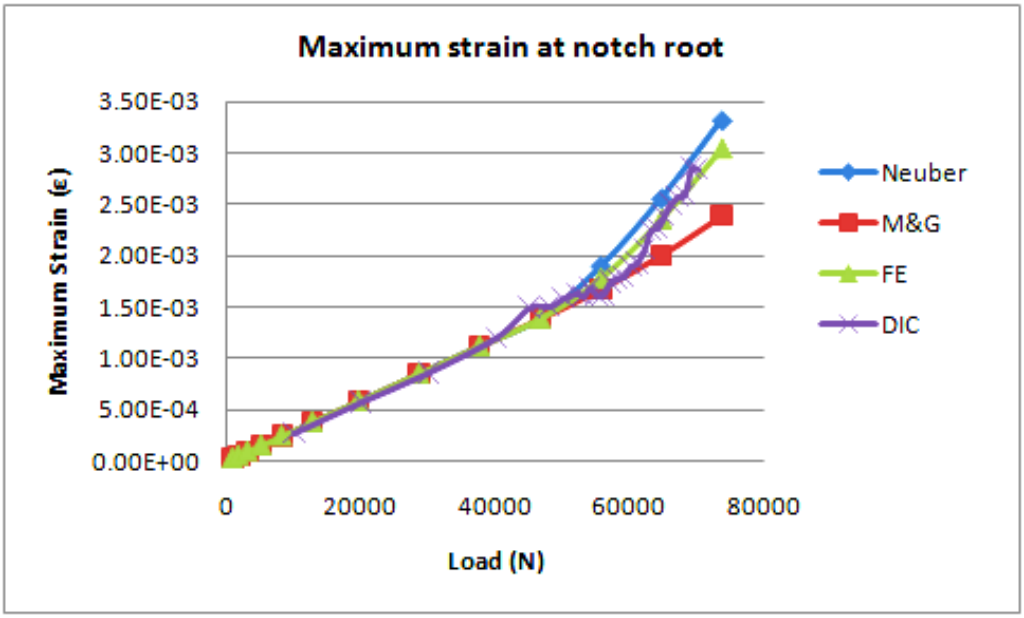

Figure 11: Maximum strain at notch root obtained by FE, DIC, Neuber and Molski & Glinka

Note the good approximation between the strains measured by the DIC system and the strains predicted by the FE analysis at the notch border. Note also that, at least for this case, Neuber's rule predictions are closer to the experimental and numerical results than the predictions made by the Molski-Glinka rule. In the linear-elastic phase, all solutions show good agreement with the DIC measured strain. From approximately 50kN, EF and Neuber present the same trending. The DIC-measured values present a slight oscillatory behavior. In spite of the irregularities, they reproduce reasonably well the FE and Neuber predictions.

6. CONCLUSIONS

DIC strain measurements in a 1020 steel plate with a central hole loaded under elastic-plastic conditions showed reasonable agreement with finite element predictions, despite the strain gradient present around the notch tip. This test demonstrates that this technique can be a practical tool for calibrating more elaborated models, a necessary step to verifying their suitability for practical applications.

7. REFERENCES

Ach, R.S., Castro Neto, J., Nóbrega, M.J.R., Castro, J.T.P. and Speranza Neto, M. "Influência da taxa de deformação nas curvas tensão×deformação de um aço 1020 pré-encruado", Anais do 65º Congresso Anual da ABM, 2010

Castro, J.T.P and Meggiolaro, M.A., 2009, "Fadiga - Técnicas e Práticas de Dimensionamento Estrutural sob Cargas Reais de Serviço: Volume I - Iniciação de Trincas", ISBN 1449514693, CreateSpace.

Shukla, A. and Dally. J.W., "Experimental Solid Mechanics", College House Enterprises, LLC, 5713 Glen Cove Drive, Knoxville Tennessee, USA, 2010.

M.A. Sutton, J.J. Orteu, H.W. Schreier, "Image Correlation for Shape, Motion and Deformation Measurements", Springer Science+Business Media, LLC, 233 Spring Street, New York, NY 10013, USA, 2009.

Yan J-H, Sutton M.A., Deng X., Cheng C-S, "Mixed mode fracture of ductile thin-sheet materials under combined in-plane and out-of-plane loading. Int J Fract 2007; 144 (4): 297-321;

8. RESPONSIBILITY NOTICE

The authors are the only responsible for the printed material included in this paper.